Icarus 454 (2026) 117075

Contents lists available at ScienceDirect

Icarus

journal homepage: www.elsevier.com/locate/icarus

Research Paper

# The rapidly evolving surface of asteroid 4 Vesta revealed by rayed craters and optical maturity

E.S. Costello [a,b,*], C.J. Tai Udovicic [a,b,c], L. Sun [a,b], P.G. Lucey [a,b]

[a] Hawaii Institute of Geophysics and Planetology, Honolulu, HI, USA
[b] University of Hawaii at Manoa, Honolulu, HI, USA
[c] University of Winnipeg, Winnipeg, MB, Canada

ARTICLE INFO

Dataset link: https://sbn.psi.edu/pds/resource/dawn/dwnvfcmosaics.html, https://sbnarchive.psi.edu/pds3/dawn/fc/DWNVSPG_2/

*Keywords:*
Vesta
Asteroids
Surfaces
Cratering
Regolith
Impact processes

ABSTRACT

We investigate the evolving surface of asteroid 4 Vesta using rayed craters and optical maturity parameters. Although largely unweathered, Vesta displays maturity anomalies in the form of bright and dark crater ray systems that contrast with the background regolith. We produced and utilized global maps of OMAT (Optical Maturity Parameter) and the Vesta-specific CC*-OMAT (Carbonaceous Chondrite OMAT), which quantitatively capture the effects of darkening and "bluing" due to the admixture of exogenic carbonaceous chondrite material, to catalog 207 OMAT-rayed craters and 165 CC*-OMAT-rayed craters. We find that rayed craters on Vesta are exceptionally ephemeral, persisting for only tens of millions of years — a lifespan of up to two orders of magnitude shorter than the roughly billion years during which rays persist on the Moon. This rapid erasure rate implies that surface processes and impact gardening on Vesta are much more intense than on the Moon. An apparent size-dependence in degradation suggests that material mixing is the dominant control on the erasure of rays, rather than an influx of carbonaceous chondrite material.

## 1. Introduction

The asteroid 4 Vesta (hereafter, "Vesta") is one of the largest objects in the asteroid belt. The mysterious space weathering story represented by Vesta was known from the dawn of planetary spectroscopy, and spectroscopy by the Dawn mission confirmed the anomaly: Vesta's surface regolith has the optical properties of unweathered regolith (Pieters et al., 2012; Blewett et al., 2016; Vdovichenko et al., 2025). Vesta was one of the first asteroids to be spectroscopically measured, and McCord et al. (1970) explicitly made the case that characteristic absorption features indicate Vesta's surface mineralogy is similar to the HED class of differentiated meteorites (Howardite, Eucrite, and Diogenite), a link supported by Earth-based spectral observations made over the following decades (McFadden et al., 1977; Binzel and Xu, 1993; Gaffey, 1997). These studies also showed Vesta to be a unique body in the space weathering story of the inner Solar System. Unlike the Moon, Mercury, Near-Earth asteroids, or Vesta's neighboring S-type asteroids, the spectra of Vesta are comparable to pristine meteorite samples in the lab without special treatment for iron-bearing space weathering products (e.g., Hiroi et al., 1994). Dawn spectral data confirmed these observations (De Sanctis et al., 2012), and showed Vesta's surface does not show evidence of extensive lunar-like space weathering (e.g., Pieters et al., 2012; Blewett et al., 2016), although there is some evidence in HED samples that limited lunar-like space weathering occurs (Noble et al., 2005).

Space weathering is the process by which the silicate surfaces of airless bodies in the Solar System are chemically and physically altered by exposure to the space environment (e.g., Pieters and Noble, 2016; Denevi et al., 2023). On the Moon, Mercury, and many S-type asteroids, space weathering exhibits a distinct spectral signature, characterized by low albedos and strong red slopes in the near-infrared (Chapman, 1996; Veverka et al., 2001; Chapman, 2004; Pieters and Noble, 2016; Denevi et al., 2023). The presence of nanophase iron has been conclusively linked to the spectral effects of lunar-like space weathering (Hapke, 2001), and analysis of the evolution of nanophase iron has been linked to aging craters (Tai Udovicic et al., 2021). Analysis of optical maturity parameters, which correlate with nanophase iron abundance (Lucey et al., 2000) has also been used to study crater evolution (e.g., Grier et al., 2001). Lunar-like space weathering is thought to be driven by a combination of the effects of solar wind and micrometeorite bombardment, and the abundance of nanophase iron has been correlated with higher solar wind irradiation, both with latitude on the Moon (Hemingway et al., 2015) and through the gradient of relative abundances from the Moon to Vesta's relatively Sun-starved neighbor asteroids (Pieters and Noble, 2016). It has also been suggested that

* Corresponding author at: Hawaii Institute of Geophysics and Planetology, Honolulu, HI, USA.
*E-mail address:* ecostello@higp.hawaii.edu (E.S. Costello).

https://doi.org/10.1016/j.icarus.2026.117075
Received 22 January 2026; Received in revised form 19 March 2026; Accepted 27 March 2026
Available online 2 April 2026

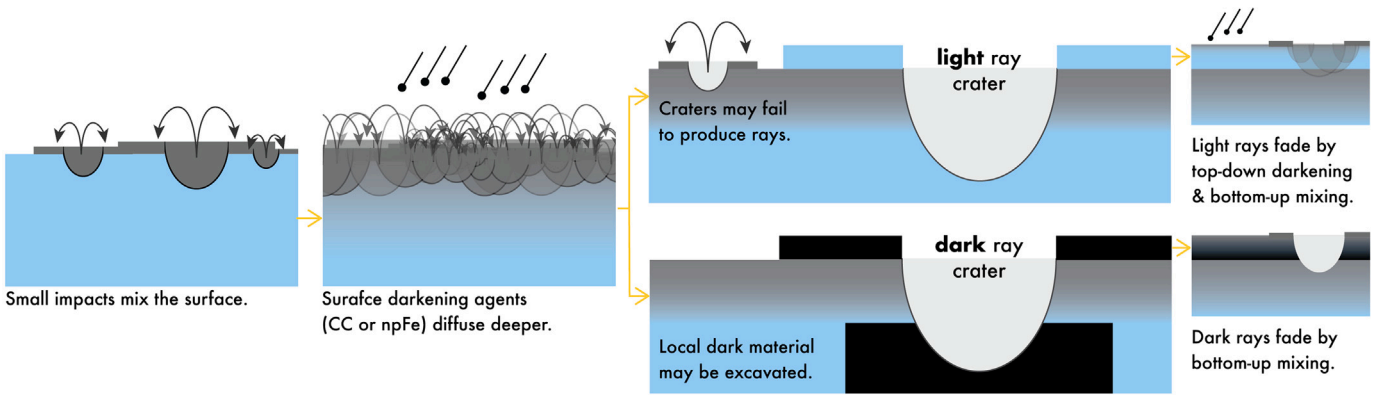


**Fig. 1.** A diagram illustrating surface evolution processes and mechanisms for how rays may form and fade.

Vesta's surface may be shielded from the solar wind by the presence of a magnetic field, much like lunar swirls (Blewett et al., 2016; Vernazza et al., 2006; Fu et al., 2012), which would produce an even more pronounced effect than latitude or distance from the Sun.

If Vesta saw no space weathering whatsoever, one would expect to observe a relatively uniform surface in spectral variability and brightness with no visible distinction between freshly excavated and ancient terrains. This is not the case. Some of Vesta's craters feature sprawling ray systems, which contrast with the background regolith both as bright and dark radial albedo patterns, while their immediate neighbors do not. Rays may have formed from the scouring of mature material from the surface and/or the deposition of relatively immature material onto the surface (Hawke et al., 2004). The more degraded state of ray-less craters relative to those with rays suggests that rays are indeed maturity anomalies (Pieters et al., 2012). Once Vestan crater rays are present at the surface, something is removing them.

It has been proposed that the combination of a rain of carbonaceous micrometeorites and impact gardening work together to mix away Vesta's crater rays (Fig. 1 Pieters et al., 2012; Reddy et al., 2012). In this study, we will show through an analysis of the abundance and distribution of rayed craters on Vesta, that intense impact mixing is the dominant surface process, and that the erosion of rays is more driven by this intense mixing with surrounding material, than by an exogenous rain of carbonaceous micrometeorites. It is relatively easy to darken light ray material by mixing in exogenic carbon (Clark, 1983), but some of Vesta's craters feature systems of dark rays. The dark rays radiating from Sossia crater, for example, will also evolve under impact gardening and dark rays must be removed by gardening with surrounding bright regolith alone — no amount of additional dark chondrites will fade them. It is possible for additional dark material to sufficiently darken the background to obscure a dark ray; however it is not reasonable on Vesta, owing to its overall high reflectivity.

Thus, material mixing must explain ray erasure. Vesta is known to have high regolith mobility driven by relatively steep topography and local gravity gradients (Pieters et al., 2012), and random mixing by impact gardening also acts to churn the surface, fading surface albedo and maturity contrasts like rays. Our analysis will show that the intensity of mixing on Vesta is dramatic in comparison to the Moon. Vestan crater rays degrade up to two orders of magnitude more rapidly than lunar crater rays.

## 2. Methods

### 2.1. Optical maturity

For space weathering of the Moon, the optical maturity parameter (OMAT) has been used to constrain the maturation of crater ejecta both from the mean OMAT of ejecta and as a function of distance from the crater rim (Lucey et al., 2000; Tai Udovicic et al., 2021; Grier et al., 2001). OMAT is correlated with lunar maturity through its sensitivity to nanophase iron content (Lucey et al., 2000). However, for this very reason, lunar-style OMAT will not fully describe maturity on Vesta. Although there is some evidence from HED samples for limited nanophase iron abundances (Noble et al., 2005), regolith maturity on Vesta is likely not dominantly reflected in nanophase iron abundance.

Vesta's surface maturity is thought to be correlated with an admixture of exogenic carbonaceous chondrite material ('CC'; Pieters et al., 2012). Blewett et al. (2016) used Dawn FC color data to define a carbonaceous chondrite optical maturity, "CC-OMAT", parameter. The CC-OMAT parameter was derived similarly to the lunar OMAT parameter, but captures maturity as it is driven by carbonaceous chondrite mixing. Model spectra show that the band ratio used to defined CC-OMAT (438/555-nm ratio and 555-nm reflectance) is positively correlated with increasing contamination with carbonaceous chondrite material (Fig. 2). Their parameter quantitatively captures the effects of CC maturity: As bright regolith matures, it becomes darker and "bluer" (i.e., the 438-nm/555-nm ratio increases).

Using radiative transfer theory, we modeled a series of spectra to replicate the space weathering effect on Vesta, observable through reflectance and reflectance ratios (Fig. 2). We adopted a howardite meteorite as the mineral end member with 54.7% orthopyroxene, 15.4% clinopyroxene, and 29.9% plagioclase. To simulate FeO variations, Mg# of this mineral was set to vary between 50 to 90 at an interval of 10 (Sun and Lucey, 2021). The darkening and reddening agent nanophase iron (Fe) is set to vary at 0.05, 0.1, 0.7, 1.0 and 5.0 wt per thousand (Hapke, 2001; Cahill et al., 2019). We also included three different contents of carbonaceous chondrite at 1%, 3% and 5% as a darkening agent on Vesta. The spectrum of the carbonaceous chondrite was obtained from Relab (Spectra ID: MB-TXH-064). A grain size of 40 μm was adopted for mineral mixture in the model. Our models show that both increasing CC and npFe effect an OMAT parameter (black arrow in Fig. 2). The CC-OMAT parameter decouples the effects of increasing npFe and increasing CC (black arrows in Fig. 2).

Using these parameter definitions, we present new global maps of OMAT and CC*-OMAT (Fig. 3) from publicly available Dawn FC2 Derived Vesta Global Mosaics v1.0 (Roatsch et al., 2015). We follow Lucey et al. (2000) in our definition of the OMAT parameter as the Euclidian distance from an mature endmember on a plot of band ratio over brightness. The origin is defined as a fixed spectral endmember at ($x_0 = 0, y_0 = 1$) because the vast majority of Dawn FC data falls below this point, establishing it as a conservative upper bound for the pure carbonaceous component. For OMAT, we chose $R_{long}$ = 965 nm, $R_{short}$ = 749 nm for the closest possible comparison with lunar OMAT, which uses 950 nm and 750 nm (Lucey et al., 2000).

$$OMAT = \sqrt{(R_{749})^2 + \left(\frac{R_{965}}{R_{749}} - 1\right)^2} \quad (1)$$

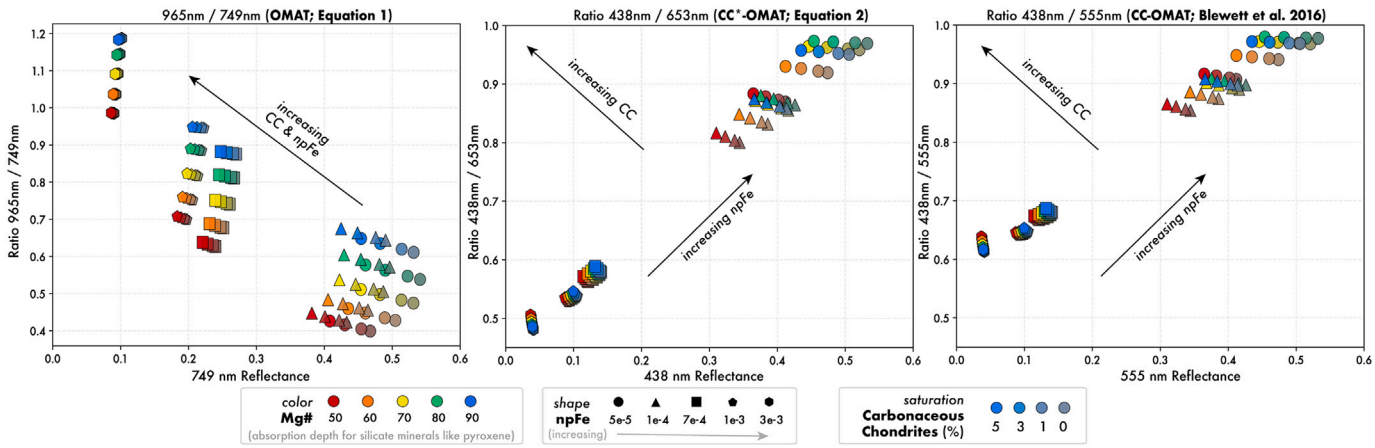


**Fig. 2.** Color ratio plots ($R_{long}/R_{long}$ versus $R_{short}$) using spectra modeled with radiative transfer theory with a howardite meteorite endmember. Left is the OMAT band ratio, center is our CC*-OMAT band ratio, and right shows minimal difference between our CC*-OMAT band ratio and the CC-OMAT band ratio presented by Blewett et al. (2016). (For interpretation of the references to color in this figure legend, the reader is referred to the web version of this article.)

To define CC*-OMAT, we follow a similar form to OMAT, but, similar to Blewett et al. (2016) CC-OMAT, we invert the long and short wavelengths in the ratio. For CC*-OMAT, we took $R_{long} = 653$ nm, $R_{short} = 438$ nm.

$$(CC^{*}-)OMAT = \sqrt{(R_{653})^2 + \left(\frac{R_{438}}{R_{653}} - 1\right)^2} \quad (2)$$

Our definition of CC*-OMAT deviates from Blewett et al. (2016) in choosing 653 nm for $R_{long}$, rather than 555 nm. This choice does not hinder the ability to distinguish contributions of CC material from nanophase iron in band ratio vs. reflectance plots; in fact, it enhances the CC-contributions to the Euclidian distance to the mature origin when npFe is lowest (Fig. 2). This change was necessary in order to avoid significant striping artifacts observed when ratioing 653 nm and 555 nm FC channels in the v1.0 Dawn Vesta global HAMO mosaics. The striping is due to imperfect calibration at image seams. It is possible these artifacts are reduced using a recently published recalibration of Dawn FC data (Kovács et al., 2024), but at the time of writing, recalibrated data are not publicly available, and reprocessing global mosaics was outside the scope of this work.

Despite the necessary changes in reflectance bands, the global maps presented here retain high fidelity to previously established measures of maturity for Vesta across diverse terrains. Following the methodology of Blewett et al. (2016), we investigate the relative maturity trajectory between pairs of proximal pixels representing "fresh" and "mature" locations. This trajectory is calculated as the distance in band-ratio-over-reflectance space for each pair to yield a fresh-to-mature distance parameter. The sign of this parameter is defined by the change in the band ratio between the two pixels (fresh minus mature), such that a positive value indicates the fresh pixel possesses a higher ratio than the mature pixel.

We extracted these values from the nearest pixels to the same 20 fresh-mature location pairs reported by Blewett et al. (2016) (see Tables 2 and 3 therein) and found that the OMAT ($R_{965}/R_{749}$ vs. $R_{749}$) and CC*-OMAT ($R_{438}/R_{653}$ vs. $R_{653}$) bands used in this study produce interpretations of maturity consistent with the CC-OMAT ($R_{438}/R_{555}$ vs. $R_{555}$) bands used in that previous work (Fig. 4). One notable exception occurs at location 16 (near Sossia crater), where the trajectory sign for both our OMAT and CC*-OMAT cases is negative rather than positive. This indicates a greater band ratio for the mature pixel relative to the fresh pixel in these specific band selections. Blewett et al. (2016) suggest that location 16 may have sampled dark mantle ejecta from the nearby Oppia crater rather than typical local background material, which likely explains the spectral divergence resulting from the choice of bands. Notably, we find that these negative values are more consistent with the weathering trends observed in 18 of the 20 other locations reported, suggesting that our band selection accurately captures the local spectral evolution.

### 2.2. Cataloging rayed craters

Using the updated maps of OMAT and CC*-OMAT, and following the methodology established for the survey of rayed craters on the Moon (Ghent et al., 2024), we cataloged all rayed craters within an area greater than 90% of the total surface of Vesta ($8.19\times10^5$ km$^2$) (Fig. 3). We identified the center latitude and longitude and the diameter of all ≥600 m diameter rayed craters. The catalog includes smaller craters, but we limit our analysis to those ≥600 m to minimize error from crater diameter approaching image resolution limits.

## 3. Results

We produced two maturity maps of Vesta (Fig. 3). The OMAT map includes lunar-style space weathering and carbonaceous chondrite material, which similarly darkens regolith. We isolate the effects of cabonasceous chondrites in the map of CC*-OMAT. The maps are similar in character at the global scale, but exhibit regional differences that track previously identified terrains on Vesta (Fig. 3). Fresh craters are observable in both maps, characterized by light ejecta and ray patterns, some of which also exhibit dark rays relative to the surrounding material. Notable differences between the two maps are associated with light mantle material, such as that near Oppia crater, which appears bright in both maps but is more evident in CC*-OMAT. Alternatively, dark mantle material (e.g., Garry et al., 2014) appears dark in OMAT, but light in CC*-OMAT (Fig. 3).

Using the OMAT and CC*-OMAT maps, we identified 207 craters with apparent rays in OMAT, and 165 craters with apparent rays in CC*-OMAT, and labeled craters that had prominent bright rays (light ray on a darker background) and dark rays (dark ray on a light background). Some craters labeled "light" or "dark" feature a mixture; however, labels were assigned based on the most prominent rays. A crater's rays could be strongly asymmetrical and still be counted within the rayed crater catalog. There are more craters with OMAT rays than craters with CC*-OMAT rays on Vesta. All craters with CC*-OMAT rays also have OMAT rays. None of the rayed craters were larger than ≈30 km diameter. As a proportion of the total crater population, rayed craters are rare. Only about 1.5% of all ≥5 km diameters craters on Vesta have rays (calculated by comparing our catalog to Liu et al. (2018), normalized to count areas).

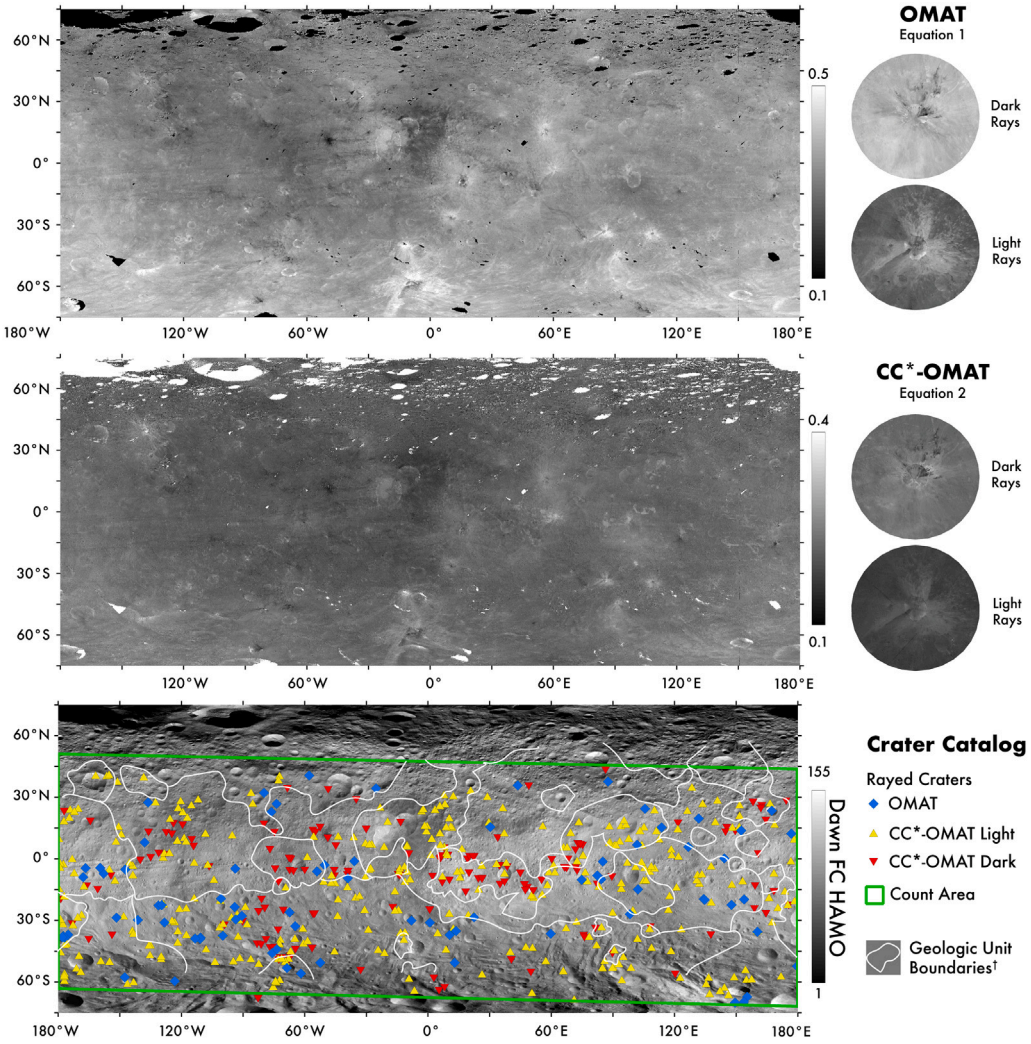


**Fig. 3.** Top: Vesta OMAT parameter; Middle: Vesta CC*-OMAT parameter; Bottom: Dawn FC HAMO mosaic and crater catalog. †Geologic unit boundaries are approximated from Yingst et al. (2023).

We contextualize our rayed crater catalog by comparing Vesta crater cumulative size-frequency distributions (CSFD; Fig. 5). The rayed crater population CSFD is plotted with regional crater populations: All craters greater than 1 to 2 km in diameter in the northern and southern hemisphere (Liu et al., 2018), craters in the northern hemisphere heavily cratered terrain (Marchi et al., 2014b), craters on the ejecta of Rheasilvia Basin (Michel et al., 2015), craters on the ejecta of Marcia crater (a 63 km diameter equatorial crater) (Michel et al., 2015), and craters on the ejecta of the rayed craters Rubria, Antonia, and Vibidia (about 10 km, 8 km, and 15 km diameters respectively) (Kneissl et al., 2014; Krohn et al., 2014). Crater location and diameter data were not publicly available for all datasets. Where crater data were not directly available (heavily cratered terrain (Marchi et al., 2014b), Rheasilvia (Michel et al., 2015), Marcia (Michel et al., 2015), Rubria, Antonia, and Vibidia (Kneissl et al., 2014; Krohn et al., 2014)), the data were digitized from published plots, and errors from both CSFD and digitization must be inferred for these comparison data.

Crater size-frequency distributions reveal information about surface evolution through changes in distribution slopes. For example, there is a downturn in the distribution of craters smaller than about 2 km in diameter counted on Rheasilvia ejecta and in the heavily cratered terrain, consistent with erasure (Fig. 5, black circles). Sufficient numbers of accumulating craters at all scales can also obliterate past craters, resulting in a characteristic "equilibrium" slope. In Fig. 5, we compare all Vestan crater populations to model crater equilibrium at 2% of geometric saturation, and 10% of geometric saturation (Gault, 1970; Costello and Lucey, 2024). At 2% of saturation, craters hundreds of meters in diameter are observed to reach equilibrium in the lunar mare (Minton et al., 2019), and equilibrium at 10% of saturation is where craters tens of kilometers in diameter are observed to reach equilibrium in the lunar highlands (Xiao and Werner, 2015). As has been suggested previously, ≥4 km diameter craters appear to be in equilibrium on Vesta (particularly in the northern hemisphere (Marchi et al., 2014a,b)).

We define surface age isochrons by combining a crater production function (Neukum et al., 2001; Bottke et al., 2020) with a chronology function (Roig and Nesvornỳ, 2020). To evaluate the age of Marcia and other rayed craters, we adopt a singular production function fit. While the geometric fit to the crater counts is relatively precise, the absolute age implied by this fit depends upon the calibration of the Rheasilvia basin anchor. Because the estimated age of Rheasilvia spans a range of 0.6 to 1.3 Ga (Bottke et al., 2020), the resulting chronological interpretation of the production function fit shifts according to the chosen anchor value. Consequently, we report our results as a systematic age range (10 to 80 Ma), corresponding to the discrete solutions obtained when the chronology function is anchored at 0.6 Ga and 1.3 Ga, respectively. This range is consistent with the 12 to 15 Ma age reported by Williams et al. (2014) and aligns with the 10–20 Ma ages observed for morphologically similar craters such as Antonia and Vibidia (Kneissl et al., 2014; Krohn et al., 2014)

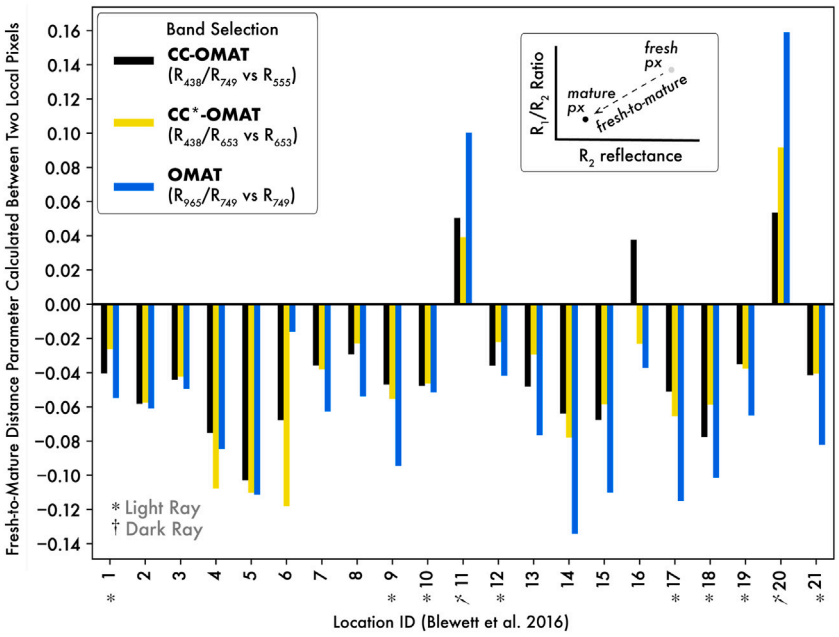


**Fig. 4.** Fresh-to-mature distance parameters across diverse Vesta locations. Data include CC-OMAT bands (black) reported by Blewett et al. (2016), alongside CC*-OMAT (yellow) and OMAT (blue) values extracted for this study. The bars show the calculated distance between a fresh point (pristine surface) and a mature point (weathered background) in spectral space. A positive value indicates the fresh point has a higher band ratio than the mature point. Conversely, a negative value (e.g., location 11) indicates the mature point has the higher ratio. Locations associated with light and dark rays are labeled for comparison. Cutout shows how the fresh-to-mature distance parameter is defined between two local fresh and mature pixels. (For interpretation of the references to color in this figure legend, the reader is referred to the web version of this article.)

The age derived from the CSFD of the ≥8 km rayed crater population yields a range that is consistent with a short ray persistence time on Vesta (≈tens of millions of years; blue dotted line in Fig. 5). This age is substantiated by the independent dating of individual prominent rayed craters within the population. Specifically, the population CSFD age range aligns with the independently determined ages of prominent rayed craters Vibidia (≈10 Ma) and Antonia (≈20 Ma) (Kneissl et al., 2014; Krohn et al., 2014). The consistency between the population age and the ages of these known-age craters reaffirms the rayed population's calculated age and indicates that Vesta's crater rays are ephemeral, lasting for only 10 to 80 million years.

## 4. Discussion

### 4.1. Space weathering on vesta

Lunar-like space weathering is suppressed on Vesta; however, more than twenty craters in our catalog appear to have rays only in OMAT, indicating some nanophase iron (npFe) production may be occurring, with the caveat that OMAT is a spectral parameter that is neatly explained by nanophase iron on the Moon, but some other phenomenon could be effecting it. If OMAT is representative of the presence of nanophase iron, then our finding agrees with previous observations that HED meteorites have revealed some grains containing npFe, indicating limited lunar-like space weathering (Noble et al., 2005).

The majority of Vesta's crater rays are apparent in CC*-OMAT, which is tuned to capture darkening by carbonaceous chondrites. The 'OMAT-only' subset disappear in this view. If limited lunar-like space weathering is occurring, it explains this discrepancy. These OMAT-only rayed craters are rare, iron-dependent maturity rays, formed by excavating relatively immature (npFe-poor) material and placing rays over relatively mature (npFe-rich) material. We therefore conclude that the spectral character of Vesta's surface experiences limited lunar-like space weathering, but dominantly 'weathers' and, more accurately, 'evolves' by the mixing of carbonaceous chondrite-rich with chondrite-poor background material, as proposed by Pieters et al. (2012).

Local deviation from global mean values of CC*-OMAT and OMAT could represent an agnostic maturity index for both light and dark-rayed craters on Vesta in future analysis. Note the differences in the magnitude of OMAT and CC*-OMAT between different rayed craters in Fig. 4. The freshest rays may exhibit a larger difference between a global mean and OMAT or CC*-OMAT, while older rays may be closer to the mean. Temporal evolution of the deviation from global mean values should also differ between light and dark rays because they are removed by parallel but distinct mechanisms. While mixing is a primary removal mechanism for both, light rays should be more sensitive to the addition of dark carbonaceous chondrite material, whereas dark rays remain relatively unaffected. We show that OMAT and CC*-OMAT are both dependent upon the Mg#, which we use to capture the absorption depth for silicate minerals like pyroxene, with the band ratio defining CC*-OMAT showing a particularly nonlinear relationship in combination with increasing npFe (Fig. 2).

In future work, with further Hapke modeling to quantify the effects of the role of pyroxene, analysis of the relative magnitude of OMAT or CC*-OMAT based on different wavelength choices (e.g., Fig. 4), a more targeted treatment of the selection of the mature origin, and our rayed crater catalog, it may be possible to quantify the rates of uniquely Vestan 'weathering', and the specific roles of local material, the input flux of carbonaceous chondrites, and mechanical material mixing. For now, we proceed to draw conclusions about the rate and magnitude of material mixing based on our catalog of craters with apparent maturity rays.

### 4.2. Rays forming and fading

Ray evolution begins with formation, which often depends on underlying geology. In our catalog, craters with prominent dark rays appear unreasonably limited in number to represent a uniform production population (i.e., not every crater makes a dark ray; Fig. 5).

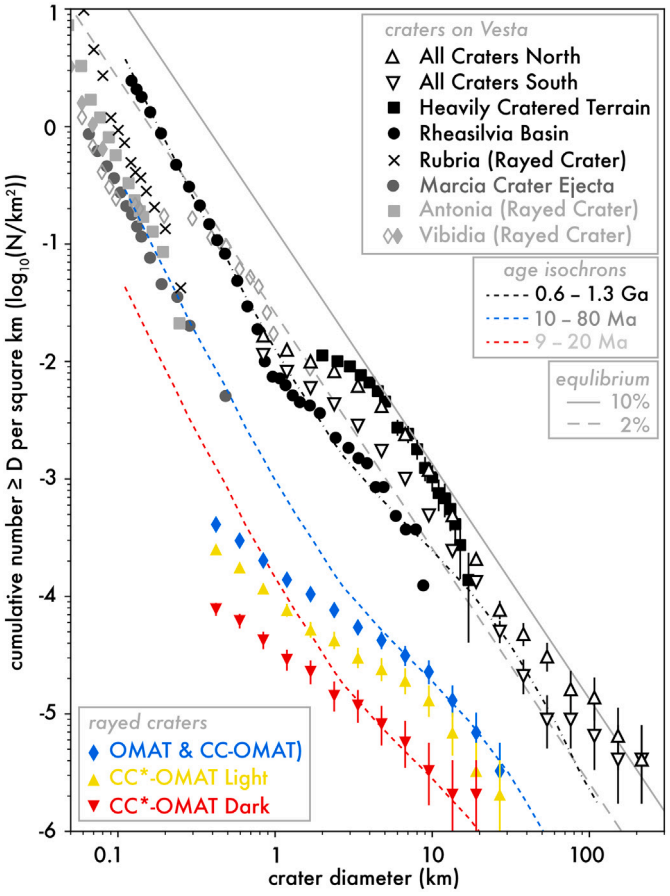


**Fig. 5.** The number of rayed craters is shown in a cumulative binned plot. Cumulative crater densities from literature are reported here for comparison (All craters larger than a kilometer diameter in the northern and southern hemispheres, Heavily Cratered Terrain, crater superposed on the ejecta of Rheasilvia Basin, and Marcia, Rubria, Antonia, and Vibidia Craters). Age isochrons are defined based on crater production (Bottke et al., 2020) and chronology functions (Roig and Nesvorný, 2020) for Vesta, anchored by the age of Rheasilvia Basin. The age range agrees with the ages inferred previously that large rayed craters (like Antonia, Rubria, and Vibidia, which are included in our rayed crater catalog) retain rays on the order of tens of millions of years. Small craters (<5 km diameter) lose their rays more quickly than large craters (>5 km diameter), as evidenced by a shallow power law slope than the crater production function. (For interpretation of the references to color in this figure legend, the reader is referred to the web version of this article.)

This suggests that local geology is a critical factor in the production of dark rays specifically. Dark rayed craters generally cluster within ejecta units of large craters like Marcia, Calpernia, and Octavia, as well as within Vestalia Terra near Cornelia and Numisia; However, the current geologic map of Vesta does not perfectly explain the production and retention of all rayed craters (Fig. 3, bottom). Because rayed craters in general occur independently of established geologic boundaries, we infer that dark rays form specifically where impacts excavate subsurface pockets of dark chondritic material.

While local geology and availability of dark material may control dark-ray formation, age ranges remain useful for establishing a lower limit to their erasure timescale. We estimate a lower limit for the age of the dark-rayed crater population by attributing the vertical offset in Crater Size-Frequency Distributions (CSFDs) entirely to age. This results in an age range between 9 and 20 Ma. This erasure timescale must be considered a lower limit because geologic context likely accounts for some of the vertical offset from which we infer age.

Evidence supports the conclusion that temporal fading more than geologic context is the dominant control on overall ray visibility. Unlike the sub-population of dark-rayed craters, the age range for the total rayed crater population aligns well with individual craters within that group (such as Vibidia and Antonia). The cumulative population of OMAT and CC*-OMAT rayed craters do not appear clustered within any specific geologic units on Vesta (Fig. 3), and craters with rays are overall rare. Rayed craters on Vesta account for only about 1% of the total population of craters (the rayed-to-not-rayed ratio for ≥5 km diameter craters is $3.17 \times 10^{-5}$ rayed craters per km$^2$ (our catalog) / $2.07 \times 10^{-3}$ craters per km$^2$ (Liu et al., 2018) = 0.015).

In our nearly global catalog of Vesta's rayed craters, there are no examples of craters whose rays, dark or light, are superposed by the ejecta of a non-rayed craters. Many craters have rays that superpose upon nearby or immediately underlying same-size or larger craters that do not have rays. If dark rays never faded, regardless of crater size or formation timescale, we would expect to see a deviation in the CSFD for dark-rayed craters compared to light-rayed craters; however, the shape of the CSFDs for both light and dark rays and the cumulative rayed crater population share similar shapes, suggesting they evolve by similar processes. The evidence, including superposition, the relative scarcity of rayed craters compared to same-sized non-rayed craters, and the overall distribution of rayed craters being independent from geologic units, supports a temporal process controlling ray visibility. We thus conclude that Vesta's crater rays characterize relatively fresh, young craters, and that these rays then fade by homogenization with the background and over a time interval consistent with the age range of the rayed crater population, 10 to 80 million years (Fig. 5).

For craters smaller than 5 km in diameter, the population deviates significantly from production isochrons. The power law slope collapses from approximately −3 to −1, implying a loss of small rayed craters from the population (Fig. 5). This size-dependency suggests that Vesta experiences intense near-surface reworking. Relatively small craters may fail to retain rays because their rays are thin and reworked rapidly into the background by a depth-limited mixing process like secondary impacts, or fail to form rays due to the presence of a thick homogenized layer (Fig. 1). A thick homogenized layer would prevent initial ray formation and accelerate ray removal. The downturn from the production isochron at about 5 km diameters suggests that the homogenized layer is on the order of hundreds of meters thick. Such a layer indicates vigorous material mixing that is one to two orders of magnitude deeper than the reworking zone on the Moon, which has only mixed regolith a meter deep in the last billion years (e.g., Costello et al., 2021).

### 4.3. Vesta's relatively rapid resurfacing

From the age of the rayed crater population, we found that the crater rays on Vesta last on the order of tens of millions of years. In contrast, on Earth's Moon, OMAT-rayed craters remain apparent and the lunar upper regolith saturates with nanophase iron after about a billion years (Grier et al., 2001; Ghent et al., 2024; Jordan et al., 2022; Tai Udovicic et al., 2021) (Fig. 6). While the global catalog of rayed craters on the Moon is only complete down to 5 km diameters (Ghent et al., 2024), it has been observed that the rays of smaller craters on the Moon also fade more quickly than their larger brethren (Lucey et al., 2000). At any size on Vesta, crater rays are up to two orders of magnitude more ephemeral than rays on the Moon (tens of millions of years versus a billion years). They also form more frequently, following the relatively high impact rate on Vesta. Craters with rays therefore both form and disappear at a rate much higher than the Moon.

The rapid erasure of rays on Vesta suggests Vesta experiences much more intense near-surface maturity-homogenizing processes than the Moon. Rays that last a billion years on the Moon are obliterated by the combined effects of nanophase iron accumulation and material mixing;

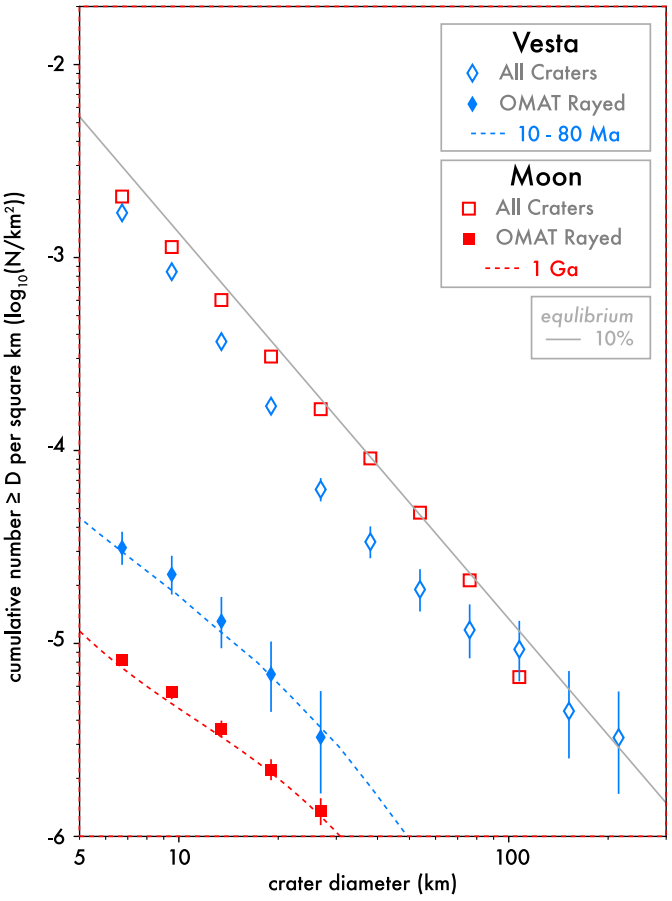


**Fig. 6.** A comparison of the crater size-frequency distributions of lunar highlands and Vestan craters and OMAT-rayed craters. Both backgrounds are near or in equilibrium (craters are sufficiently numerous and overlapping to erase). Isochrons and age ranges are defined for Vesta here as they were in Fig. 5. Note the dramatic difference in chronology, driven by the higher recent impact rate on Vesta. A 100 million year-old surface on Vesta is more cratered than a 1 billion year old surface on the Moon. Background craters on Vesta are from Liu et al. (2018). Background craters on the Moon are from Robbins (2019), normalized to the count area of the lunar highlands. Lunar OMAT-rayed raters are from the catalog by Ghent et al. (2024), also normalized to the lunar highlands count area.

however, Vesta experiences limited lunar-like space weathering. On Vesta, intense material mixing must explain the majority of ray erasure.

Boulders on Vesta (10 m scale) have surface lifetimes of approximately 300 My (Schröder et al., 2021), which is comparable to 1 m-scale boulders on the Moon (Basilevsky et al., 2015). These similar lifetimes at different spatial scales do not imply equivalent surface evolution. Because smaller, catastrophic impacts are exponentially more frequent than larger ones, 10 m boulders should persist much longer than 1 m boulders. Similar degradation rates therefore suggest that Vesta's size-normalized breakdown is significantly faster: it requires a high frequency of large-scale impacts to match the Moon's small-scale impact rate. While we refrain from calculating a precise relative impact rate, noting that breakdown may also depend on thermal stresses (Molaro et al., 2017) and distinct material properties (e.g., Rüsch and Aussel, 2024; Chertok et al., 2023), the observed rock breakdown rate supports the hypothesis that Vesta undergoes rapid surface evolution driven by intense impact bombardment.

### 4.4. The mechanisms of mixing

Mass movement can be driven by impact gardening or mass wasting, both of which likely contribute to the erasure of rays on Vesta. Vesta is known to have high regolith mobility driven by relatively steep topography and local gravity gradients (Pieters et al., 2012). Mass wasting features, such as slumps and landslides, are widespread on Vesta, particularly at steep scarps and crater rims (Kneissl et al., 2014; Krohn et al., 2014). Further, smooth, flat dust pond deposits have been observed on Vesta, indicating the movement of fines by seismic shaking or volatile-induced fluidization. If mass wasting is the dominant driver of the homogenization of Vesta's surface and fading of rays, we should observe fewer rayed craters in regions with dramatic topography, like the Divalia Fossae region around the equator; however, the spatial distribution of rayed craters appears independent of previously defined geologic units (Fig. 3), and we observe rays to follow radial patterns seemingly independent from local slopes (Fig. 7). Mass wasting is locally intense (e.g., slumps and landslides), and may more quickly destroy portions of individual craters' ray systems, resulting in asymmetrical craters and ray systems; however, craters were included in our catalog even if their rays were asymmetrical. Thus, we can conclude that while local mass wasting likely contributes to local ray erasure, it cannot explain the erasure of widespread ray systems globally.

The global, pervasive destructive processes necessary to remove craters' entire ray systems on Vesta is therefore likely impact-related mixing. Impacts contribute to mass movement on asteroids through the stochastic process of impact gardening. However, modeling this process accurately has proven challenging. For instance, a theoretical model for Vesta's neighbor, Ceres, predicted much shallower and less intense gardening than what is observed on the Moon (Costello et al., 2021). This prediction contradicts observations of near-surface ice and the mixing of organics on million-year timescales, which both suggest significantly more intense, larger-scale gardening is occurring (e.g., Prettyman et al., 2021; De Sanctis et al., 2024). The primary limitation of the model of gardening on Ceres was its chosen crater production function. The production function was extrapolated from the distribution of all craters on Ceres, a population likely in equilibrium, similar to Vesta's, and used high-error estimates for the production of secondary craters. Equilibrium masks a true, larger impactor population, as equilibrium is defined to occur when craters are actively removed from a crater population. To accurately model impact gardening on either Ceres or Vesta, a more realistic crater production function and a corresponding chronology function are required, particularly for the smallest sizes which drive gardening (≤1 km diameter). These models must also be validated against cumulative crater size-frequency distributions on smaller scales and younger surfaces, such as the CSFDs we collected from the ejecta of Marcia, Antonia, and Vibidia (Fig. 5). Further, although Ceres' surface features rayed craters (e.g., Stephan et al., 2019; Nathues et al., 2016), no Ceres-specific catalog of rayed craters collected from an optical maturity dataset or albedo map yet exists for direct comparison to our Vesta catalog.

While a suitable production function for dating craters on asteroids like Vesta is available (Bottke et al., 2020), a reliable chronology function to scale the impact rate over time is also necessary. Impact gardening is a function of time and must follow the cratering rate, which itself changes. Existing studies of crater chronology on Vesta are not suitable for this purpose, as they focus on primordial events like the Late Heavy Bombardment rather than the recent impact rate relevant to surface evolution over tens of millions of years (e.g., Schmedemann et al., 2014; Marchi et al., 2014b; de Elia and Di Sisto, 2011). Compounding this problem, analytic forms of chronology functions for Vesta are not publicly available. A valuable future step would be to extract analytic forms for both production and chronology functions from numerical models of bodies in the asteroid belt. This would be analogous to the widely used 12th-order polynomial production function and chronology functions that are standard for the Inner Solar

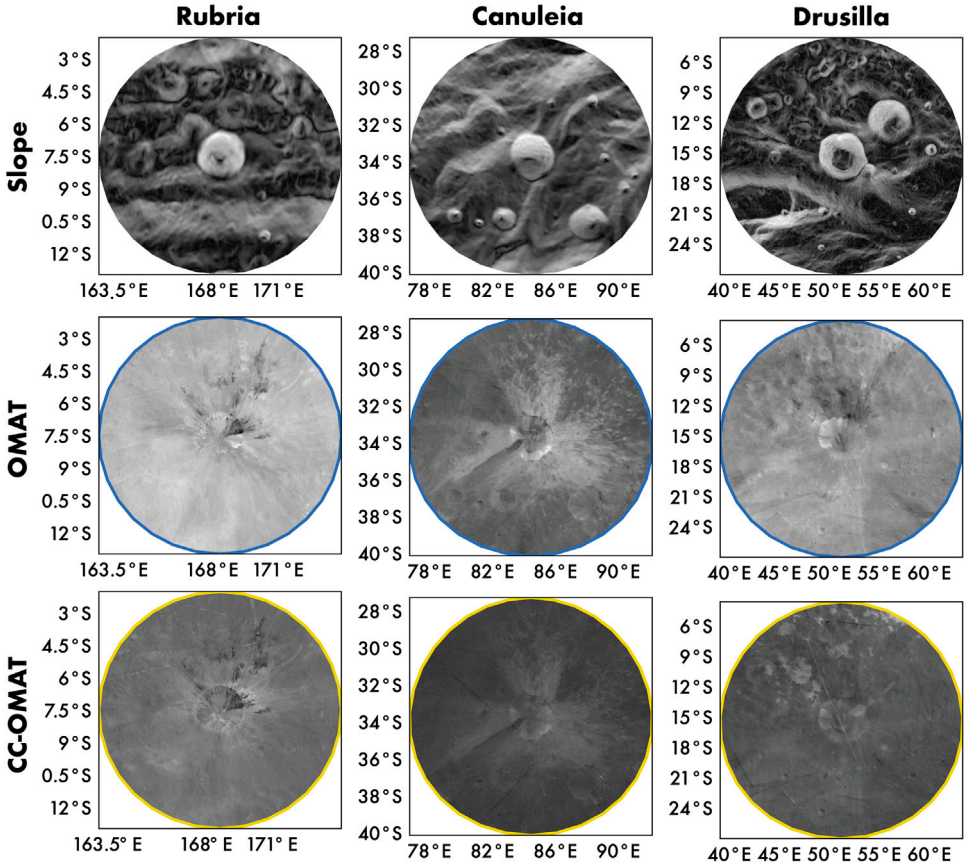


**Fig. 7.** Radial ray patterns appear independent of slope, as is demonstrated in these three named crater examples. The top row is a slope map derived from the Vesta digital terrain model (Preusker et al., 2016), the middle row is our derived OMAT, and the bottom row is our derived CC*-OMAT. Craters were included in our catalog, even if their rays were asymmetrical, mitigating the effects of local mass wasting on our analysis of ray erasure.

System (Neukum et al., 2001). Developing such analytical forms would enable consistent, comparable age-dating methodologies, drastically improving models and interpretations of the rates, drivers, and effects of surface processes on asteroids. Understanding chronology and crater production functions is particularly important, as the relatively high rate of impact bombardment on Vesta compared to the Moon is likely a direct driver of the relatively high rates of impact gardening.

Tied to the primary impact rate and chronology is secondary crater production. Secondary impacts may be prolific on Vesta, mixing the uppermost surface over tens of million year timescales with sufficient vigor to homogenize the light and dark contrasts of rays. Crater distributions interpreted to be shaped by secondaries have been widely observed (see, for example, the steep slopes of the CSFD of hundred-of-meters diameter craters in Fig. 5, Williams et al. (2014), Schmedemann et al. (2014), Krohn et al. (2014) and Marchi et al. (2014a)). The secondaries of Rheasilvia basin have been hypothesized to have scoured the troughs of Divalia Fossae (Hirata, 2023), although recent work points towards a tectonic origin (Cheng et al., 2025).

Secondaries may be more abundant than previously thought, and rays may also be thinner on Vesta than on higher-gravity bodies like the Moon, both of which contribute to rapid ray fading. Although Vesta's relatively low escape velocity suggests more secondaries might be lost to space compared to the Moon, its primary impact velocities are also lower (Blewett et al., 2016). This lower primary impact energy means fewer ejected particles reach escape velocity, allowing more to re-impact the surface. The balance may therefore result in more numerous widespread secondaries. If rays are uniformly thinner, perhaps due to Vesta's low gravity and secondary dispersion causing longer ejecta run-out distances, we would likely see more rapid erasure overall, as thin layers are more vulnerable to disruption and mixing by exponentially more numerous small impacts. However, uniformly thinner rays alone cannot explain the accelerated, size-dependent erasure we observed for the rays of craters smaller than 5 km in diameter. Ongoing and future work on the retention of secondary crater-forming debris and ejecta mobility on Vesta will be illuminating (e.g., Zeilnhofer, 2025), particularly regarding how secondaries contribute to both the formation and subsequent rapid erasure of crater rays.

## 5. Conclusions

We investigated the surface evolution of asteroid 4 Vesta, as revealed by the abundance of rayed craters and optical maturity. Two new maps of optical maturity (OMAT and CC*-OMAT) revealed hundreds of craters with prominent rays. All rays apparent in CC*-OMAT are also apparent in OMAT, and a limited number of rays are apparent only in OMAT, indicating that limited but non-zero lunar-like space weathering occurs and some nanophase iron-related maturity contrasts exist on Vesta. Using the catalog of rayed craters, we assessed the age of the rayed crater population and interpreted the shape of the crater size-frequency distributions to determine the likely drivers of surface evolution on Vesta.

The rays of large craters (≥5 km diameter) on Vesta only persist for tens of millions of years. This lifespan is dramatically short, making Vesta's rays up to two orders of magnitude more ephemeral than those on the Moon, where rays can remain apparent for about a billion years. This rapid rate of erasure necessitates the conclusion that surface processes at the scale of crater rays on Vesta are much more intense than on the Moon, despite relatively limited nanophase iron production and lunar-style space weathering.

Pervasive, global erasure of rays, especially the dark rays that cannot be erased by admixture with in-falling carbonaceous material, points strongly to random mass transport/mixing as the dominant mechanism over the long term. Mass wasting may act as an intensifier, but since localized mass wasting features cannot explain the globally random ray distribution, the most probable pervasive, stochastic mixing mechanism must be intense impact gardening, which is highly effective at shallow depths.

To fully understand the rate and actors in the apparent rapid and random mass transport on Vesta, be they primary or secondary impacts, we must better constrain and communicate understanding of the recent and relatively small impact rate (the last billion years, and less than 10 km crater diameter scales). As a foundational step, developing analytic forms for both the production and chronology functions, analogous to the standard Inner Solar System models, will be critical for enabling consistent, comparable age-dating methodologies and accurately interpreting the rates of surface processes on asteroids and dwarf planets.

## CRediT authorship contribution statement

**E.S. Costello:** Writing – review & editing, Writing – original draft, Visualization, Validation, Supervision, Software, Resources, Project administration, Methodology, Investigation, Funding acquisition, Formal analysis, Data curation, Conceptualization. **C.J. Tai Udovicic:** Writing – review & editing, Validation, Software, Formal analysis, Data curation. **L. Sun:** Writing – review & editing, Software, Methodology, Formal analysis. **P.G. Lucey:** Writing – review & editing, Validation, Formal analysis.

## Declaration of competing interest

The authors declare that they have no known competing financial interests or personal relationships that could have appeared to influence the work reported in this paper.

## Acknowledgments

This work was supported by a NASA Discovery Data Analysis program grant (80NSSC24K0065).

## Data availability

Dawn FC mosaic and DTM data are available on the PDS, and can be accessed at the following links (FC: https://sbn.psi.edu/pds/resource/dawn/dwnvfcmosaics.html; DTM: https://sbnarchive.psi.edu/pds3/dawn/fc/DWNVSPG_2/). Crater shapefiles, point queries for Fig. 4 and the images in Fig. 7 were collected using the Craterpy Python package (Tai Udovicic et al., 2025). The Vesta rayed crater catalog is archived on Zenodo (Costello (2026)).

## References

Basilevsky, A., Head, J., Horz, F., Ramsley, K., 2015. Survival times of meter-sized rock boulders on the surface of airless bodies. Planet. Space Sci. 117, 312–328.
Binzel, R.P., Xu, S., 1993. Chips off of asteroid 4 vesta: Evidence for the parent body of basaltic achondrite meteorites. Science 260 (5105), 186–191.
Blewett, D.T., Denevi, B.W., Le Corre, L., Reddy, V., Schröder, S.E., Pieters, C., Tosi, F., Zambon, F., De Sanctis, M.C., Ammannito, E., et al., 2016. Optical space weathering on Vesta: Radiative-transfer models and Dawn observations. Icarus 265, 161–174.
Bottke, W., Vokrouhlickỳ, D., Ballouz, R.-L., Barnouin, O., Connolly, H., Elder, C., Marchi, S., McCoy, T., Michel, P., Nolan, M., et al., 2020. Interpreting the cratering histories of Bennu, Ryugu, and other spacecraft-explored asteroids. Astron. J. 160 (1), 14.
Cahill, J.T., Blewett, D.T., Nguyen, N.V., Boosalis, A., Lawrence, S.J., Denevi, B.W., 2019. Optical constants of iron and nickel metal and an assessment of their relative influences on silicate mixture spectra from the FUV to the NIR. Icarus 317, 229–241.
Chapman, C.R., 1996. S-type asteroids, ordinary chondrites, and space weathering: The evidence from Galileo's fly-bys of Gaspra and Ida. Meteorit. Planet. Sci. 31 (6), 699–725.
Chapman, C.R., 2004. Space weathering of asteroid surfaces. Annu. Rev. Earth Planet. Sci. 32 (1), 539–567.
Cheng, H.C.J., Klimczak, C., Matsuyama, I., 2025. Reorientation and despinning of 4 Vesta formed the Divalia Fossae. Sci. Adv. 11 (26), eads7984.
Chertok, M.A., Lucey, P.G., Costello, E.S., Ireland, S.M., 2023. The rock abundance of crater populations as a probe of mare protolith properties. J. Geophys. Res.: Planets 128 (7), e2023JE007767.
Clark, R.N., 1983. Spectral properties of mixtures of montmorillonite and dark carbon grains: Implications for remote sensing minerals containing chemically and physically adsorbed water. J. Geophys. Res.: Solid Earth 88 (B12), 10635–10644.
Costello, E., 2026. Vesta rayed craters catalog. http://dx.doi.org/10.5281/zenodo.18332361.
Costello, E., Ghent, R., Lucey, P., 2021. Impact gardening on Ceres. Geophys. Res. Lett. 48 (8), e2021GL092960.
Costello, E., Lucey, P., 2024. The age and evolution of lunar micro cold traps at the scale of surface exploration. Geophys. Res. Lett. 51 (1), e2023GL105369.
de Elia, G.C., Di Sisto, R.P., 2011. Impactor flux and cratering on Ceres and Vesta: implications for the early solar system. Astron. Astrophys. 534, A129.
De Sanctis, M., Ammannito, E., Capria, M., Tosi, F., Capaccioni, F., Zambon, F., Carraro, F., Fonte, S., Frigeri, A., Jaumann, R., et al., 2012. Spectroscopic characterization of mineralogy and its diversity across Vesta. Science 336 (6082), 697–700.
De Sanctis, M.C., Baratta, G.A., Brucato, J.R., Castillo-Rogez, J., Ciarniello, M., Cozzolino, F., De Angelis, S., Ferrari, M., Fulvio, D., Germanà, M., et al., 2024. Recent replenishment of aliphatic organics on Ceres from a large subsurface reservoir. Sci. Adv. 10 (39), eadp3664.
Denevi, B.W., Noble, S.K., Christoffersen, R., Thompson, M.S., Glotch, T.D., Blewett, D.T., Garrick-Bethell, I., Gillis-Davis, J.J., Greenhagen, B.T., Hendrix, A.R., et al., 2023. Space weathering at the Moon. Rev. Miner. Geochem. 89 (1).
Fu, R.R., Weiss, B.P., Shuster, D.L., Gattacceca, J., Grove, T.L., Suavet, C., Lima, E.A., Li, L., Kuan, A.T., 2012. An ancient core dynamo in asteroid Vesta. Science 338 (6104), 238–241.
Gaffey, M.J., 1997. Surface lithologic heterogeneity of asteroid 4 Vesta. Icarus 127 (1), 130–157.
Garry, W.B., Williams, D.A., Yingst, R.A., Mest, S.C., Buczkowski, D.L., Tosi, F., Schäfer, M., Le Corre, L., Reddy, V., Jaumann, R., et al., 2014. Geologic mapping of ejecta deposits in Oppia Quadrangle, Asteroid (4) Vesta. Icarus 244, 104–119.
Gault, D.E., 1970. Saturation and equilibrium conditions for impact cratering on the lunar surface: Criteria and implications. Radio Sci. 5 (2), 273–291.
Ghent, R.R., Costello, E.S., Parker, A., 2024. The population of young craters on the moon: New catalog and spatial and temporal analysis. Planet. Sci. J. 5 (4), 89.
Grier, J.A., McEwen, A.S., Lucey, P.G., Milazzo, M., Strom, R.G., 2001. Optical maturity of ejecta from large rayed lunar craters. J. Geophys. Res.: Planets 106 (E12), 32847–32862.
Hapke, B., 2001. Space weathering from Mercury to the asteroid belt. J. Geophys. Res.: Planets 106 (E5), 10039–10073.
Hawke, B.R., Blewett, D.T., Lucey, P.G., Smith, G., Bell III, J.F., Campbell, B.A., Robinson, M.S., 2004. The origin of lunar crater rays. Icarus 170 (1), 1–16.
Hemingway, D.J., Garrick-Bethell, I., Kreslavsky, M.A., 2015. Latitudinal variation in spectral properties of the lunar maria and implications for space weathering. Icarus 261, 66–79.
Hirata, N., 2023. Secondary cratering from Rheasilvia as the possible origin of Vesta's equatorial troughs. J. Geophys. Res.: Planets 128 (3), e2022JE007473.
Hiroi, T., Pieters, C., Takeda, H., 1994. Grain size of the surface regolith of asteroid 4 Vesta estimated from its reflectance spectrum in comparison with HED meteorites.
Jordan, A., Shusterman, M., Tai Udovicic, C., 2022. Modeling the production of submicroscopic iron in the lunar highlands. Icarus 387, 115184. http://dx.doi.org/10.1016/j.icarus.2022.115184.
Kneissl, T., Schmedemann, N., Reddy, V., Williams, D., Walter, S., Neesemann, A., Michael, G., Jaumann, R., Krohn, K., Preusker, F., et al., 2014. Morphology and formation ages of mid-sized post-Rheasilvia craters–Geology of quadrangle Tuccia, Vesta. Icarus 244, 133–157.
Kovács, G., Nathues, A., Sierks, H., Gutiérrez Marqués, P., Hoffmann, M., Thangjam, G.S., 2024. The scientific calibration of the dawn framing camera. Space Sci. Rev. 220 (1), 4.
Krohn, K., Jaumann, R., Elbeshausen, D., Kneissl, T., Schmedemann, N., Wagner, R., Voigt, J., Otto, K., Matz, K.-D., Preusker, F., et al., 2014. Asymmetric craters on vesta: Impact on sloping surfaces. Planet. Space Sci. 103, 36–56.
Liu, Z., Yue, Z., Michael, G., Gou, S., Di, K., Sun, S., Liu, J., 2018. A global database and statistical analyses of (4) Vesta craters. Icarus 311, 242–257.
Lucey, P.G., Blewett, D.T., Taylor, G.J., Hawke, B.R., 2000. Imaging of lunar surface maturity. J. Geophys. Res.: Planets 105 (E8), 20377–20386.
Marchi, S., Bottke, W., O'Brien, D., Schenk, P., Mottola, S., De Sanctis, M., Kring, D., Williams, D., Raymond, C., Russell, C., 2014a. Small crater populations on Vesta. Planet. Space Sci. 103, 96–103.
Marchi, S., Morbidelli, A., Bottke, W.F., Schenk, P.M., Russell, C.T., Raymond, C.A., et al., 2014b. Constraining the cratering chronology of Vesta. Planet. Space Sci. 103, 131–142.

McCord, T.B., Adams, J.B., Johnson, T.V., 1970. Asteroid Vesta: Spectral reflectivity and compositional implications. Science 168 (3938), 1445–1447.
McFadden, L.A., McCord, T.B., Pieters, C., 1977. Vesta: The first pyroxene band from new spectroscopic measurements. Icarus 31 (4), 439–446.
Michel, P., DeMeo, F.E., Bottke, W.F., 2015. Asteroids IV. University of Arizona Press.
Minton, D.A., Fassett, C.I., Hirabayashi, M., Howl, B.A., Richardson, J.E., 2019. The equilibrium size-frequency distribution of small craters reveals the effects of distal ejecta on lunar landscape morphology. Icarus 326, 63–87.
Molaro, J.L., Byrne, S., Le, J.-L., 2017. Thermally induced stresses in boulders on airless body surfaces, and implications for rock breakdown. Icarus 294, 247–261.
Nathues, A., Hoffmann, M., Platz, T., Thangjam, G., Cloutis, E., Reddy, V., Le Corre, L., Li, J.-Y., Mengel, K., Rivkin, A., et al., 2016. FC colour images of dwarf planet ceres reveal a complicated geological history. Planet. Space Sci. 134, 122–127.
Neukum, G., Ivanov, B.A., Hartmann, W.K., 2001. Cratering records in the inner solar system in relation to the lunar reference system. In: Chronology and Evolution of Mars: Proceedings of an ISSI Workshop, 10–14 April 2000, Bern, Switzerland. Springer, pp. 55–86.
Noble, S.K., Keller, L.P., Pieters, C., 2005. Evidence of space weathering in regolith breccias I: Lunar regolith breccias. Meteorit. Planet. Sci. 40 (3), 397–408.
Pieters, C., Ammannito, E., Blewett, D., Denevi, B., De Sanctis, M., Gaffey, M., Le Corre, L., Li, J.-Y., Marchi, S., McCord, T., et al., 2012. Distinctive space weathering on vesta from regolith mixing processes. Nature 491 (7422), 79–82.
Pieters, C., Noble, S., 2016. Space weathering on airless bodies. J. Geophys. Res.: Planets 121 (10), 1865–1884.
Prettyman, T.H., Yamashita, N., Landis, M.E., Castillo-Rogez, J.C., Schörghofer, N., Pieters, C., Sizemore, H.G., Hiesinger, H., Marchi, S., McSween, H.Y., et al., 2021. Replenishment of near-surface water ice by impacts into Ceres' volatile-rich crust: Observations by Dawn's gamma ray and neutron detector. Geophys. Res. Lett. 48 (15), e2021GL094223.
Preusker, F., Scholten, F., Matz, K.-D., Roatsch, T., Jaumann, R., Raymond, C., Russell, C., 2016. Dawn FC2 Derived Vesta DTM SPG V1.0. NASA Planetary Data System, Dataset ID: DAWN-A-FC2-5-VESTADTMSPG-V1.0.
Reddy, V., Le Corre, L., O'Brien, D.P., Nathues, A., Cloutis, E.A., Durda, D.D., Bottke, W.F., Bhatt, M.U., Nesvorny, D., Buczkowski, D., et al., 2012. Delivery of dark material to vesta via carbonaceous chondritic impacts. Icarus 221 (2), 544–559.
Roatsch, T., Kersten, E., Matz, K.-D., Preusker, F., Scholten, F., Elgner, S., Schroeder, S., Jaumann, R., Raymond, C., Russell, C., 2015. Dawn FC2 derived vesta global mosaics V1. 0. NASA Planet. Data Syst. 252, DAWN–A.
Robbins, S.J., 2019. A new global database of lunar impact craters > 1–2 km: 1. Crater locations and sizes, comparisons with published databases, and global analysis. J. Geophys. Res.: Planets 124 (4), 871–892.
Roig, F., Nesvornỳ, D., 2020. Modeling the chronologies and size distributions of Ceres and Vesta craters. Astron. J. 160 (3), 110.
Rüsch, O., Aussel, B., 2024. The evolution of rock size-frequency distribution on the Moon: Effects of rock strength and fragmentation products on centimeter-scale abundances. J. Geophys. Res.: Planets 129 (10), e2024JE008626.
Schmedemann, N., Kneissl, T., Ivanov, B., Michael, G., Wagner, R., Neukum, G., Ruesch, O., Hiesinger, H., Krohn, K., Roatsch, T., et al., 2014. The cratering record, chronology and surface ages of (4) Vesta in comparison to smaller asteroids and the ages of HED meteorites. Planet. Space Sci. 103, 104–130.
Schröder, S.E., Carsenty, U., Hauber, E., Schulzeck, F., Raymond, C.A., Russell, C.T., 2021. The boulder population of asteroid 4 Vesta: Size-frequency distribution and survival time. Earth Space Sci. 8 (2), e2019EA000941.
Stephan, K., Jaumann, R., Zambon, F., Carrozzo, F., Wagner, R., Longobardo, A., Palomba, E., De Sanctis, M., Tosi, F., Ammannito, E., et al., 2019. Ceres' impact craters–Relationships between surface composition and geology. Icarus 318, 56–74.
Sun, L., Lucey, P.G., 2021. Unmixing mineral abundance and Mg# with radiative transfer theory: modeling and applications. J. Geophys. Res.: Planets 126 (2), e2020JE006691.
Tai Udovicic, C., Costello, E., Ghent, R., Edwards, C., 2021. New constraints on the lunar optical space weathering rate. Geophys. Res. Lett. 48 (14), e2020GL092198.
Tai Udovicic, C., Essunfeld, A., Costello, E., 2025. Craterpy: Impact crater data science in Python. J. Open Source Softw. 10 (113), 8663. http://dx.doi.org/10.21105/joss.08663.
Vdovichenko, V., Teifel, V., Kharitonova, G., 2025. Asteroid 4 vesta: from ground observations to the Dawn Mission–Evolution of concepts of mineralogical composition and surface structure. Sol. Syst. Res. 59 (5), 53.
Vernazza, P., Brunetto, R., Strazzulla, G., Fulchignoni, M., Rochette, P., Meyer-Vernet, N., Zouganelis, I., 2006. Asteroid colors: a novel tool for magnetic field detection? The case of vesta. Astron. Astrophys. 451 (3), L43–L46.
Veverka, J., Thomas, P., Robinson, M., Murchie, S., Chapman, C., Bell, M., Harch, A., Merline, W., Bell III, J., Bussey, B., et al., 2001. Imaging of small-scale features on 433 Eros from NEAR: Evidence for a complex regolith. Science 292 (5516), 484–488.
Williams, D.A., Denevi, B.W., Mittlefehldt, D.W., Mest, S.C., Schenk, P.M., Yingst, R.A., Buczkowski, D.L., Scully, J.E., Garry, W.B., McCord, T.B., et al., 2014. The geology of the Marcia quadrangle of asteroid vesta: Assessing the effects of large, young craters. Icarus 244, 74–88.
Xiao, Z., Werner, S.C., 2015. Size-frequency distribution of crater populations in equilibrium on the moon. J. Geophys. Res.: Planets 120 (12), 2277–2292.
Yingst, R.A., Mest, S.C., Garry, W.B., Williams, D.A., Berman, D.C., Gregg, T.K., 2023. A geologic map of vesta produced using a hybrid method for incorporating spectroscopic and morphologic data. Planet. Sci. J. 4 (9), 157.
Zeilnhofer, M.F., 2025. The preliminary investigation of impact craters on asteroid (4) Vesta. Space Educ. Strateg. Appl. 5 (2).